Int. J. Electrochem. Sci., 17 **(2022)** Article Number: 220666, doi: 10.20964/2022.06.63

International Journal of
ELECTROCHEMICAL
SCIENCE
www.electrochemsci.org

Large-scale and One-step Synthesis of CoP/NC as a Highly Active Electrocatalyst for the Hydrogen Evolution Reaction and Oxygen Reduction Reaction

Haodong Zhou, Jingyi Zhao, Qidi Wu, Weijun Li[*]*, Jing Tang*[*]

School of Mechanical Engineering, Liaoning Petrochemical University, No. 1, Dandong Road, Fushun 113001, Liaoning, China
[*]E-mail: fstangcandy@126.com ; lijuanw123@163.com

Received: 20 February 2022 / *Accepted:* 13 April 2022 / *Published:* 7 May 2022

For clean and renewable energy research, developing non-noble metal electrocatalysts with high activity and stability for the hydrogen evolution reaction (HER) and oxygen reduction reaction (ORR) is critical. Herein, cobalt phosphide/N-doped carbon (CoP/NC) was synthesized by an extremely convenient approach. Compared with pure CoP, NC wrapped around CoP nanoparticles, which prevented the agglomeration and improved electron transfer of CoP. The obtained CoP/NC exhibited better activity than pure CoP, which has a low overpotential (η_{10}=139/248 mV) and a small Tafel slope (59/82 mV dec^{-1}) in 0.5 M H_2SO_4 and 1 M KOH for the HER. CoP/NC exhibited excellent stability with no obvious change in activity for the HER after 5000 cycles. CoP/NC also had high ORR activity, which gave a more positive half-potential (0.85 V) and onset potential (0.9 V) than pure CoP at 1600 rpm in 0.1 M KOH.

Keywords: CoP/NC, one step synthesis, hydrogen evolution reaction, oxygen reduction reaction

1. INTRODUCTION

As energy demands and environmental awareness in the world continue to rise, hydrogen and air batteries are highly regarded as environmentally friendly attractive fuel alternatives to traditional fossil fuels because they are environmentally friendly and have high effective capacity.[1, 2] Among various methods for producing hydrogen, electrochemical water splitting is a desirable and efficient technique.[3, 4] Although Pt and Pt alloys demonstrate favorable activity for the hydrogen evolution reaction (HER)[2, 5, 6] and oxygen reduction reaction (ORR), commercial applications are not feasible due to their high price and scarcity.[7, 8] Given this limitation, electrocatalysts with high abundance and low cost must urgently be developed for the HER and ORR.

Among these non-precious metal materials, transitional metal phosphides (TMPs)[9–12] are considered the most promising candidates for the HER and ORR as a result of their high electrocatalytic performance in acidic and alkaline media. For the same TMPs, P-rich TMPs may offer better electrocatalytic performance because phosphorus in metal phosphides can attract electrons from metal atoms and improve corrosion resistance, leading to high activity.[13, 14] However, if the P content increases, the P atoms will greatly inhibit the electron delocalization of metal atoms, which will decrease conductivity and lead to slow electrochemical HER kinetics.[13, 15] Nevertheless, key parameters affecting catalytic activity are associated with the electrical conductivity and exposed active sites.[16–18] Many efforts have been devoted to improve the conductivity of TMPs.[19–21] To improve the HER and ORR, carbon-based materials can be doped with heteroatoms.[22, 23] The nitrogen doping of carbon-based materials is particularly useful for facilitating the HER and ORR.[23, 24] In carbon substrates doped with nitrogen, the adjacent carbon atoms are stimulated to generate a positive charge density, resulting in effective catalytic active sites.[25, 26]

For instance, Shi and co-workers demonstrated that CoP@FeCoP/nitrogen-doped carbon (NC) shows a low overpotential (η_{10}=141) and high stability for the HER.[27] Ma and co-workers prepared CoP@NC by using polyaniline, showing superior electrochemical activity for the HER, which has a small overpotential (η_{10}=135 mV) and a low Tafel slope (59.3 mV dec^{-1}) in 0.5 M H_2SO_4.[28] Nevertheless, the preparation processes of these nanocatalysts are complicated and time-consuming. Developing CoP on heteroatom-doped carbon materials at a large scale is necessary to make practical applications possible, but the task remains extremely challenging.

In this work, a one-step synthesis of CoP/NC was reported, which is generally suitable for industrial scale-up. The NC network acted as a support layer on top of CoP, thereby enhancing conductivity and preventing CoP from agglomeration and dissolution. CoP/NC demonstrated high activity for the HER with a low overpotential (η_{10}=139 mV) and a small Tafel slope (59 mV dec^{-1}), as well as high stability with no obvious attenuation after 5000 cycles in acidic media. In addition, CoP/NC presented excellent ORR performance in 0.1 M KOH, and the ORR of CoP/NC was the main $4e^-$ reaction.

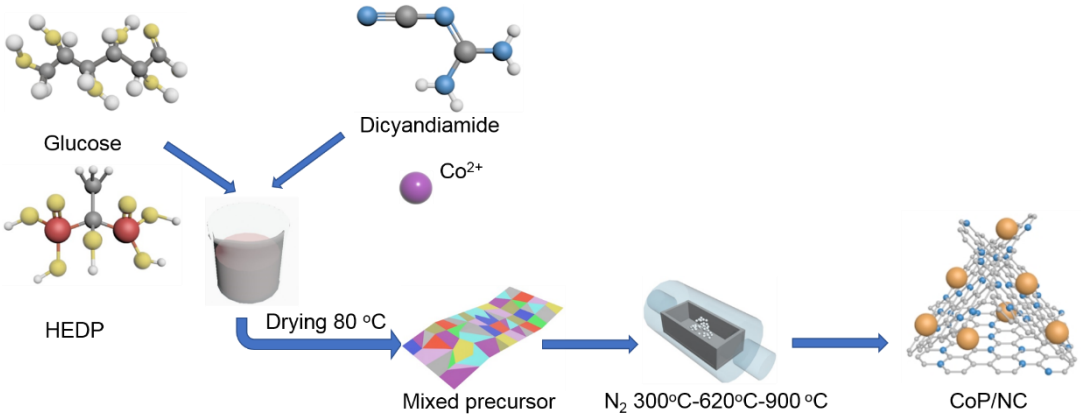

Figure 1. Schematic illustration of synthesis process of CoP/NC

2. EXPERIMENTAL

2.1. Preparation of CoP/NC

In brief, 0.2 g of $Co(NO_3)_2 \cdot 6H_2O$ (Aladdin, AR,99%) and 4 g of $C_2H_4N_4$ (Aladdin, AR, 99%) were sonicated into 150 mL of deionized water, followed by the addition of 50 mL of mixed solution of 1 g of $C_6H_{12}O_6$ (Aladdin, AR, 99%) and 0.1 g of $C_2H_8O_7P_2$ (Aladdin, AR, 99%) to form a transparent solution for 1 h. The mixed solution was stirred at 80 °C until solid mixtures were obtained. The precursor powder was then carbonized at 350 °C for 0.5 h, 620 °C for 2 h, and 900 °C for 0.5 h under N_2 atmosphere at a heating rate of 3 °C min^{-1}. The NC and pure CoP were prepared following a similar method but with $Co(NO_3)_2$ and $C_2H_4N_4$/$C_6H_{12}O_6$ as precursors.

2.2. Material characterization

X-ray diffraction (XRD) patterns were registered by XRD (BRUKER D8 ADVANCE) with Cu Kα radiation (λ=1.5406 Å). The structural morphology of catalysts was obtained by scanning electron microscopy (SEM; SEM SU8010). Transmission electron microscopy (TEM) and high-resolution TEM (HRTEM) were carried out on JEM-2100F transmission electron microscope. The surface elemental composition and bonding configuration of the samples were detected by X-ray photoelectron spectrometry (XPS; ESCALAB). The functional groups on the surface of the samples were determined with Fourier transform infrared spectroscopy (FTIR; Thermo Scientific, NICOLET iS50 FT-IR).

2.3. Electrochemical measurements

All electrochemical measurements were carried out in a three-electrode system in 0.5 m H_2SO_4 or 1 M KOH using CHI660e potentiostat in three-electrode configuration for the HER. The working electrode was a catalyst film-coated glassy carbon electrode; a graphite rod was used as the counter, and a saturated calomel electrode (SCE) was used as the reference electrode. About 4 mg of catalysts was redispersed in a mixture solvent containing 12.5 μL of Nafion (5 wt.%), 990 μL of ethanol (98 vol.%) and water. The as-prepared mixture was sonicated for 30 min thoroughly to form a homogeneous ink. For comparison, commercial Pt/C (20 wt.%) and pure CoP and NC catalyst inks were also prepared with the same method. All the potentials in this work were iR converted to the reversible hydrogen electrode by $E_{RHE}=E_{SCE}+0.0591\times pH$. The SCE was also referenced to the RHE, as shown in Figure S5. Linear sweep voltammetry (LSV) was carried out at a scan rate of 5 mV s^{-1}. Electrochemical impedance spectroscopy (EIS) was conducted at an overpotential of 100 mV in a frequency range from 100 kHz to 0.1 Hz with an AC perturbation of 5 mV. The electrochemically active surface area (ECSA) of samples was quantified by cyclic voltammetry (CV) at various scanning rates from 10 mV s^{-1} to 100 mV s^{-1} in the non-Faradaic region between 0.1 and 0.2 V (vs. RHE). The long-term durability was examined by CV at a scanning rate of 200 mV s^{-1} and by using chronoamperometry at a current density of 10 $mAcm^{-2}$.

The ORR performance of samples was carried out in a three-electrode system in 0.1 M KOH in three-electrode configuration. The working electrode was a catalyst film-coated glassy carbon electrode with 0.17 mg·cm^{-2}; a Pt wire was used as the counter, and SCE was used as the reference electrode. The LSV curves were measured in O_2-saturated 0.1 M KOH solution at 800, 1200, 1600, and 2000 rpm at a scan rate of 10 mV s^{-1} over the potential range from 1.1 V to 0 V. The measured background current was subtracted in N_2-saturated electrolyte. The number of electrons transferred per oxygen molecule was obtained by the Koutecky–Levich equation:

$$J^{-1} = J_k^{-1} + (B\omega^{1/2})^{-1} \quad (1)$$

$$\mathrm{B} = 0.62\mathrm{nF}(D_{O_2})^{2/3}\vartheta^{-1/6}C_{O_2} \quad (2)$$

where J is the current density, J_k is the kinetic current density, J_L is the limiting diffusion current density, ω is the electrode rotating rate, F is Faraday constant (96,485 C mol^{-1}), n is the number of electrons transferred per oxygen, D_{O_2} is the diffusion coefficient of O_2 in 0.1 M KOH (1.9×10^{-5} cm^2·s^{-1}), υ is the kinematic viscosity of 0.1 M KOH (0.01 cm^2·s^{-1}), and C_{O_2} is the bulk concentration of dissolved O_2 (1.2×10^{-6} mol·cm^{-3}).

3. RESULTS AND DISCUSSION

The schematic preparation process for CoP/NC with $Co(NO_3)_2$, $C_6H_{12}O_6$, $C_2H_8O_7P_2$(HEDP), and $C_2H_4N_4$ as precursors is illustrated in Figure 1. $C_2H_4N_4$ served as a nitride source, which bonded with the carbon source by donor–acceptor interactions, facilitating the generation of NC networks.[29, 30] $C_2H_8O_7P_2$ as an organic phosphorus source was mixed uniformly with $C_6H_{12}O_6$ and $C_2H_4N_4$, and $Co(NO_3)_2$ was added in the mixture. The Co ion was complexed with the phosphate group, resulting in the in situ generation of CoP, which was enveloped by NC, thereby impeding the occurrence of agglomeration under high temperature treatment. The reaction process was demonstrated by thermogravimetric analysis (TGA) as shown in Figure S1. The g-C_3N_4 nanosheets were obtained at 350 °C,[31] and CoP was synthesized and NC networks were simultaneously formed by decomposing C_3N_4 at 600 °C–700 °C.[32]

XRD further showed the generation of CoP/NC (Figure 2a). A diffraction peak at 26.5° was correlated with the (002) plane of graphite carbon, and six other peaks of CoP at 2θ=31.5°, 36.5°, 46.3°, 48.1°, and 56.9° were associated with the (011), (111), (112), (211), and (103) planes of CoP species, respectively.[33, 34] The broad peak between 20° and 30° corresponded to the (002) plane of graphitic carbon.[19, 35] Compared with pure CoP, CoP/NC (Figure 2c) was irregularly shaped, and its size was smaller than pure CoP (Figure 2b). The TEM images (Figures 2d and 2e) of CoP, CoP/NC, and NC (Figure S2) showed that some nanoparticles were wrapped with the NC networks. HRTEM characterization showed that 0.283 (Figure 2f) and 0.25 nm (Figure S3b) matched well with the (011) and (200) planes of CoP, respectively, implying that CoP was wrapped with NC networks, which limited the growth and agglomeration of the CoP particles.[36]

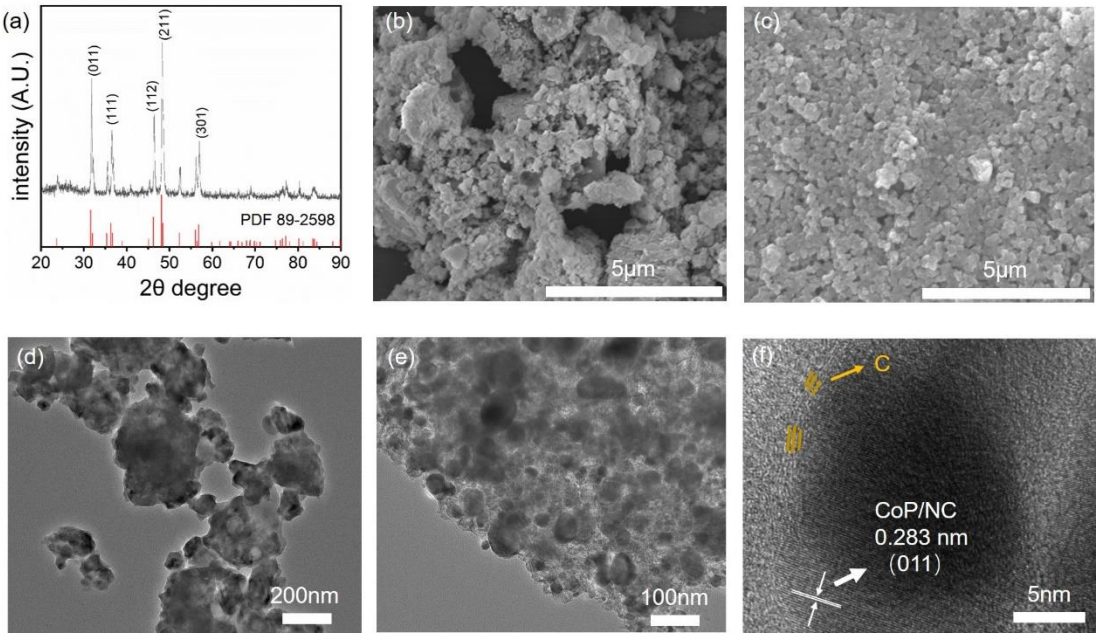

Figure 2. The XRD of the CoP/NC (a), the SEM of the pure CoP (b) and CoP/NC (c), and the TEM of the pure CoP (d) and CoP/NC (e,f)

XPS was conducted to examine the chemical composition of CoP/NC. As shown in Figure S4a, the entire XPS spectrum (CoP/NC) contained elements of C, Ni, O, and P. The XPS spectrum of Co 2p in Figure S4b showed two peaks assigned to the Co-P bond of CoP at 779.8 and 795.1 eV.[3, 19] The other peaks at 781.6 and 798.3 eV corresponded to Co-O due to the oxidation of the Co surface in CoP.[37] The peaks at 129.6 and 133.6 eV from the P 2p spectrum (Figure S4c) were attributed to the P-Co[28, 38] bond of CoP and the P-O bond.[39] These results were in accordance with the findings of XRD, indicating that CoP was obtained. Two peaks at 395.6 and 401 eV in the N 1s spectrum (Figure S4d) corresponded to pyrrolic N and graphitic N, respectively.[29, 40] The spectra of C 1s (Figure S4e) exhibited three main peaks at 284.7, 285.8, and 288.4 eV, respectively, which corresponded to C-C, N-C, and O-O. These results demonstrated that N was doped into the C network.

To further study the performance, the hydrogen evolution reactions were performed in acid and alkaline solution. Linear sweep voltammetry (LSV) was corrected (Figure S5). In Figure 3a, LSVs show that the overpotential of Pt/C was close to 30 mV. The overpotential of CoP/NC was lower (η_{10}=139 mV) than that of pure CoP and NC, demonstrating that CoP/NC had high hydrogen evolution activity. The incorporation of the NC network had a positive effect on the performance of CoP due to the high conductivity of NC, and it impeded the agglomeration and growth of CoP. CoP/NC still displayed high catalytic activity compared with the other catalysts in Table 1. In addition, the electrocatalytic kinetics of samples were evaluated by Tafel slope. The three reaction steps in acid solution were Volmer (120 mV dec^{-1}), Heyrovsky (40 mV dec^{-1}), and Tafel (30 mV dec^{-1}). The slope of CoP/NC in Figure 3b (59 mV dec^{-1}) was much smaller than that of CoP and NC, revealing high electrocatalytic kinetics for the HER and Volmer–Heyrovsky pathway for CoP/NC. EIS and CV were performed to investigate the high electrocatalytic mechanism. The Nyquist plots shown in Figure 3d demonstrated that the diameter of the semicircle of CoP/NC was much smaller than that of the NC network and pure CoP, suggesting high

electron transfer. Double-layer capacitance (C_{dl}) via CV curves (10–100 mV s^{-1}; Figure S6) was used to estimate ECSA, given that C_{dl} is linearly proportional to ECSA. Figure 3c shows that the C_{dl} value of CoP/NC was 34 mF/cm^2, which was much higher than that of pure CoP (0.16 mF/cm^2), corresponding to high HER activity because of the decrease in particle size.

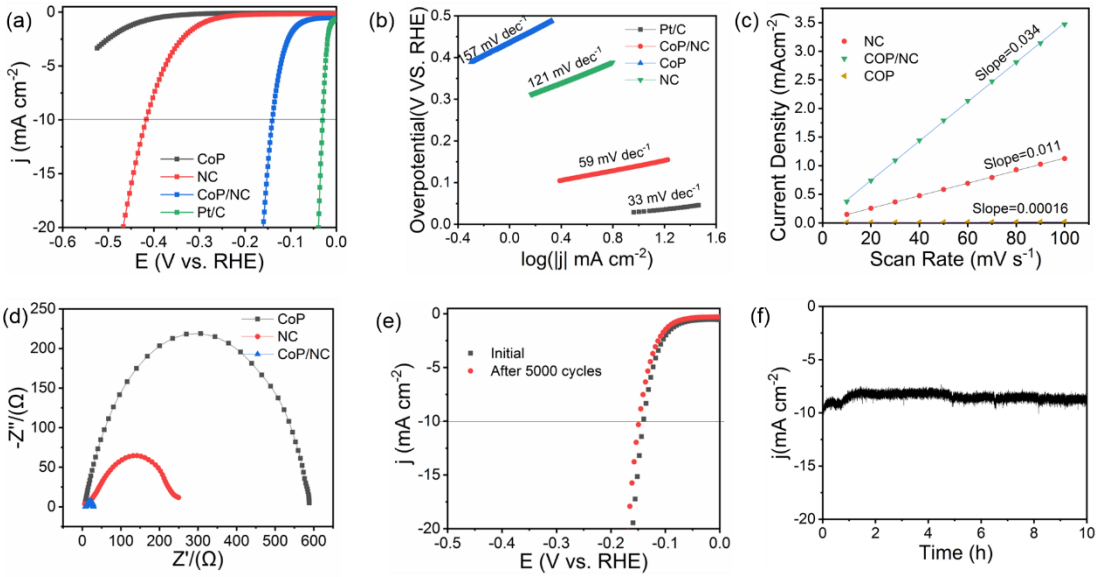

Figure 3. (a) LSV and (b) Tafel plots of CoP/NC, CoP and NC; (c) Relatioship between the current densities and scanning rates in the CV curves of CoP/NC, CoP and NC; (e) Nyquist plots of CoP/NC, CoP and NC; (f) Polarization curves of CoP/NC before and after 5000 cycles and i-t curve of CoP/NC.

Table 1. Comparison of the performance of representative precious CoP HER electrocatalysts.

Electrodes	Media	HER Overpotentials (mV) (10 mA cm^{-2})	HER Tafel Slopes (mV dec^{-1})	Catalyst loading (mg cm^{-2})	References
CoP	0.5 M H_2SO_4	139	59	0.28 mg	Our work
CoP/CN@ MoS_2	0.5 M H_2SO_4	144	69	0.255	[41]
CoP@C nanocables	0.5 M H2SO4	170	61	0.353	[42]
CoP–CNTs	0.5 M H_2SO_4	139	52	---	[43]
CoP/C-120	0.5 M H_2SO_4	286	219	---	[44]
CoP NPs	0.5 M H_2SO_4	214	73	---	[45]
CoP–RGO	0.5 M H_2SO_4	156.9	70.22	0.285	[46]
CoP-NS/C	0.5 M H_2SO_4	140	59	0.14	[38]
CoP-350	0.5 M H_2SO_4	126	64	0.45	[47]
CoP-400	0.5 M H_2SO_4	208	86	0.45	[47]
CoP-MnP	0.5 M H_2SO_4	203.1	88.2	0.354	[48]

The electrochemical stability of CoP/NC is also an important parameter to evaluate the electrochemical performance for the HER. Figure 3e shows that the activity of CoP/NC showed no significant modifications before and after 5000 cycles. The durability of CoP/NC was also determined by chronopotentiometry. Figure 3f illustrates that the current density of CoP/NC showed no obvious debasement. Thus, CoP/NC presented excellent durability and stability for the HER due to NC's

protection, which could impede nanoparticle dissolution. CoP/NC also showed high activity (η_{10}=248 mV), Tafel slope of 82 mV dec^{-1}, and good stability with no obvious change after 3000 cycles (Figure S7) in 1 M KOH.

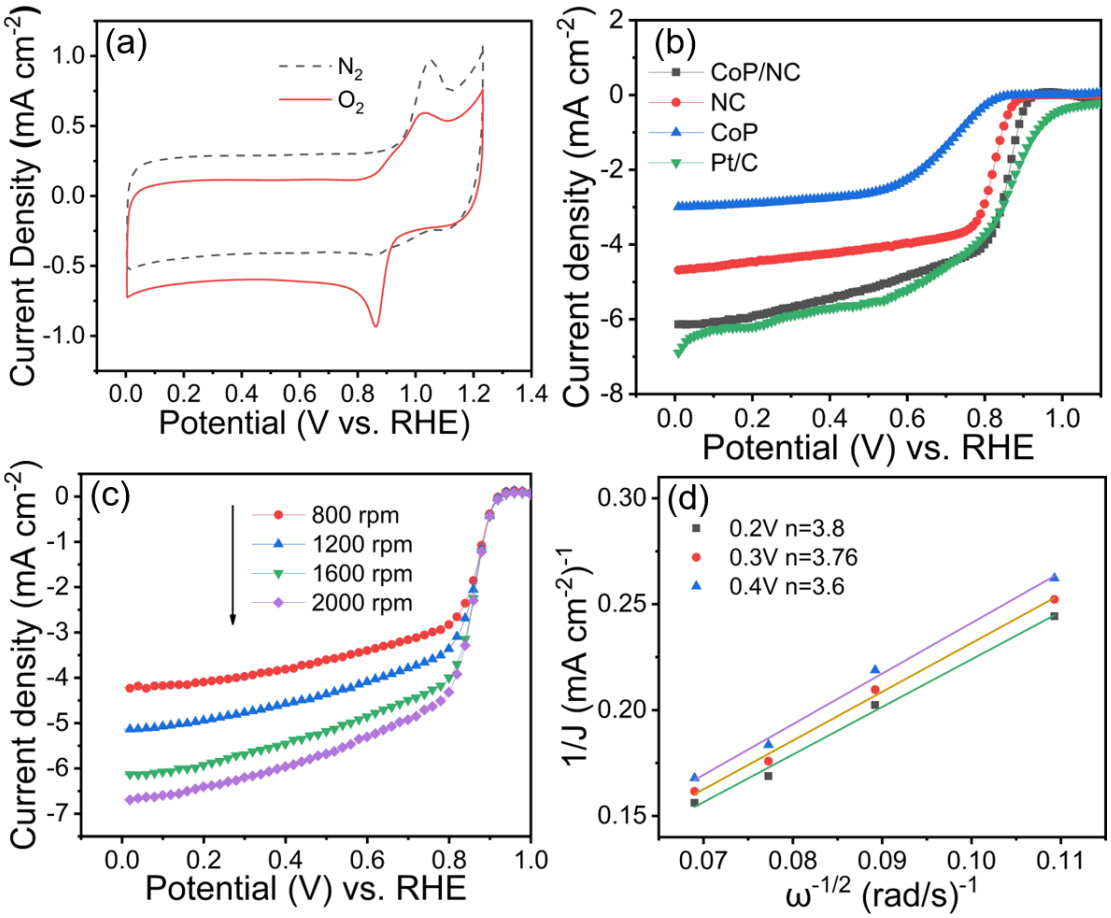

Figure 4. (a) Cyclic voltammetry of CoP/NC in N_2-and O_2-saturated 0.1 M KOH solutions and (b) LSV of CoP/NC, CoP, Pt/C and NC at 1600 rpm; (c) LSV curves of CoP/NC at 800, 1200, 1600 and 2000 rpm. (d) The K-L plots of CoP/NC at 0.2, 0.3 and 0.4 V.

Figure 4a shows the CV curves for CoP/NC in N_2- or O_2-saturated 0.1 M KOH solution, which strongly suggested the activity of CoP/NC for ORR. LSVs (Figure 4b) were employed to study the ORR performance of CoP/NC, CoP, NC, and Pt/C within 0.1 M KOH at 1600 rpm using rotating disk electrodes (RDEs). The onset potential (E_{onset}) and half-potential ($E_{1/2}$) of CoP/NC (0.9 and 0.85 V, respectively) were lower than those of Pt/C (1.0 and 0.87 V, respectively) and higher than those of CoP (0.8 and 0.67 V, respectively) and NC (0.88 and 0.82 V, respectively). The high electrocatalytic activity of CoP/NC for ORR was due to the high conductivity of the NC network and N doping, which could promote the adsorption of ORR intermediates and impede the growth of CoP. The LSV of CoP/NC at different rotational speeds in Figure 4c revealed that J_L increased with increasing rotation speed, suggesting the kinetic controlled process of ORR. Koutecky–Levich (K–L) at 0.2, 0.3, and 0.4 V from RDE polarization shown in Figure 4d presented excellent linearity based on the first reduction. According to the K–L plots, the calculated number of electron transfer was about 3.8–3.6, similar to the value of Pt/C. Thus, the process of CoP/NC was beneficial to the 4e- pathway to create H_2O or two-

electron (2e-) pathway to create H_2O_2 and subsequently reduced to H_2O. However, CoP and NC displayed poor ORR performance, revealing that the $2e^-$ oxygen reduction formed H_2O_2 (Figure S8).

4. CONCLUSION

In conclusion, CoP NC was successfully synthesized via a straightforward one-step synthetic approach. The obtained CoP NC demonstrated outstanding electrocatalytic properties. The CoP NC for the HER displayed a low overpotential (η_{10}=139 mV) and small Tafel slope (59 mV dec^{-1}) and superior stability with almost no change after 5000 cycles in H_2SO_4 due to the protection of the highly conductive NC network wrapping the CoP nanoparticles. In addition, the CoP NC for ORR exhibited higher activity (E_{onset}=0.85 V, $E_{1/2}$=0.9 V) than pure CoP and NC. The reduction process for ORR was through the $4e^-$ pathway. This simple approach is expected to be applied to the synthesis of other phosphides for the industrialization of free Pt catalyst.

SUPPORTING INFORMATION:

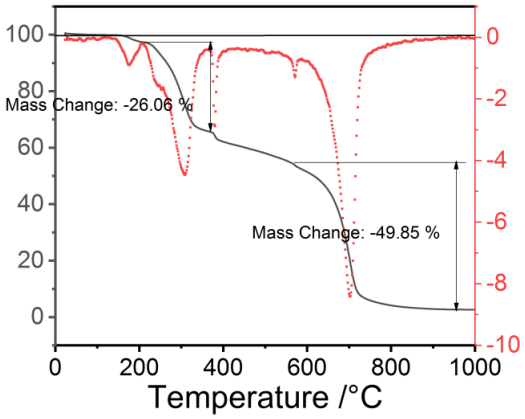

Figure S1. TGA curve of CoP/NC.

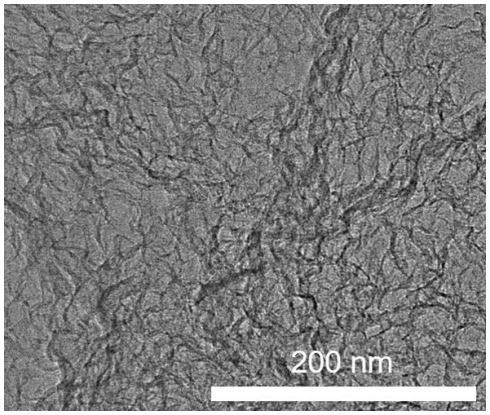

Figure S2. TEM image of the NC.

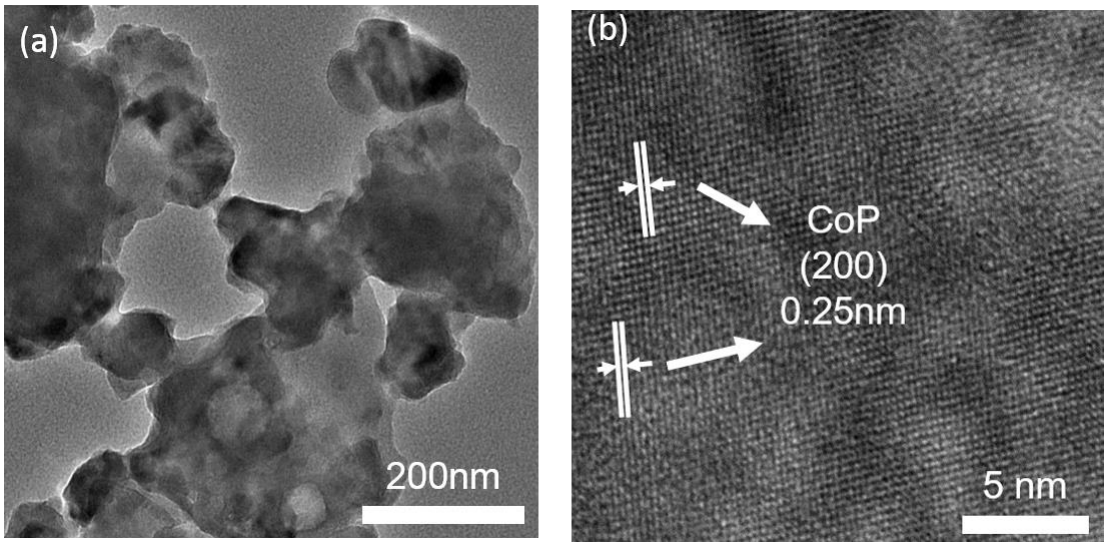

Figure S3. TEM (a) and HRTEM (b) images of the pure CoP.

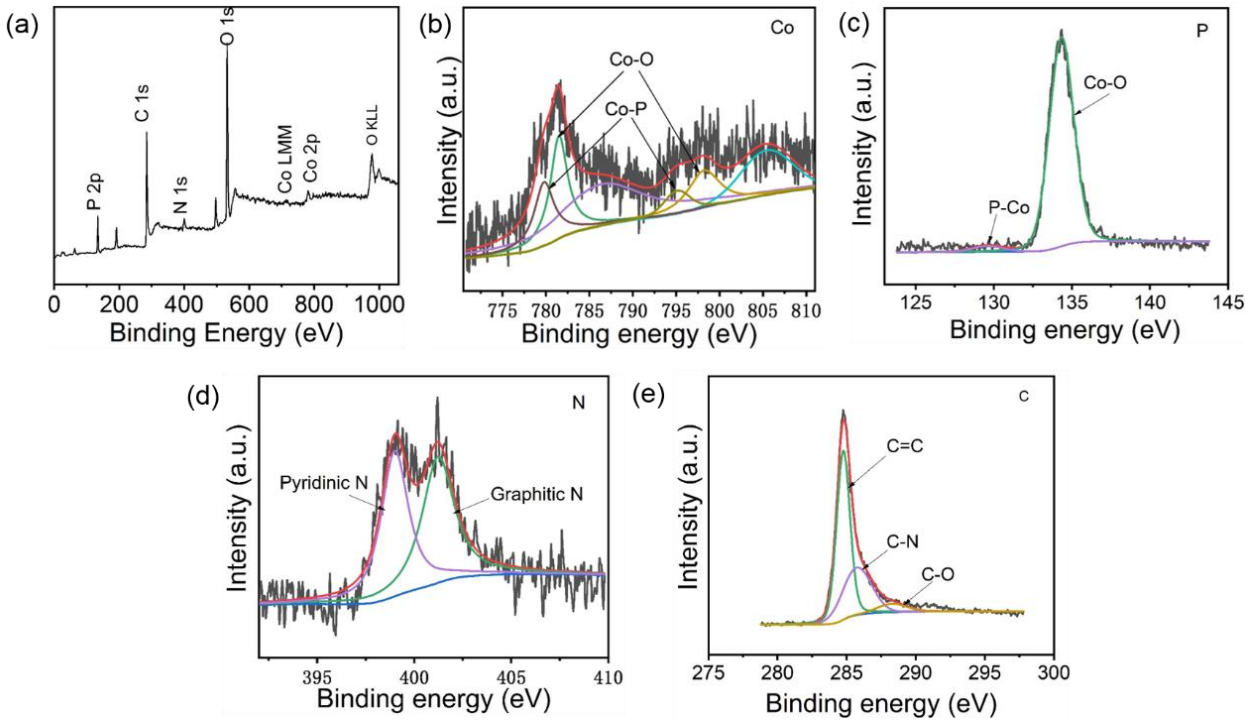

Figure S4. The XPS survey (a) and the related high resolution XPS Co 2p (b), P 2p (c), N 1s (d), C 1s (e) spectrum of CoP/NC.

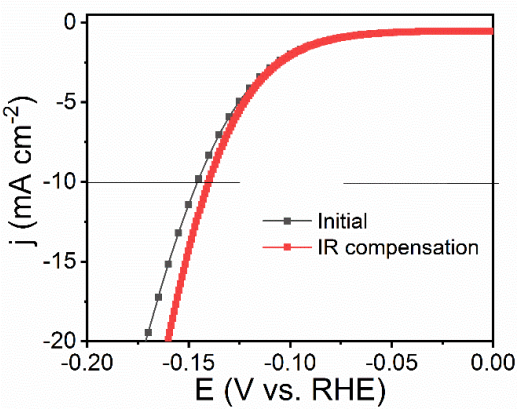

Figure S5. LSV curves of the CoP/NC in 0.5 M H_2SO_4 with and without iR correction.

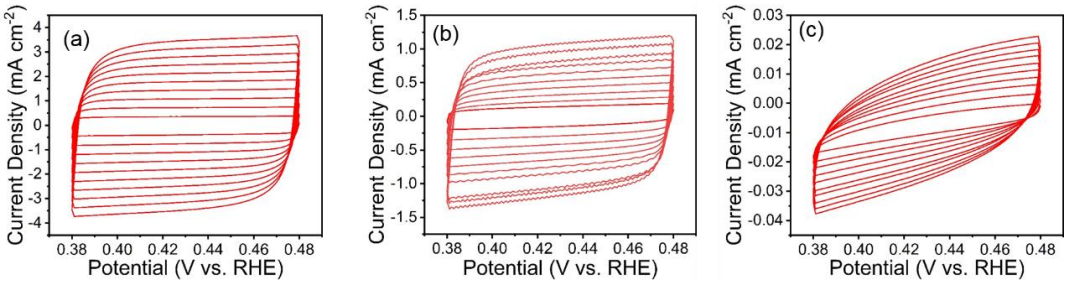

Figure S6. CV curves of (a) CoP/NC, (b) NC, and (c) pure CoP at different scanning rates from 10 to 100 mV s^{-1}.

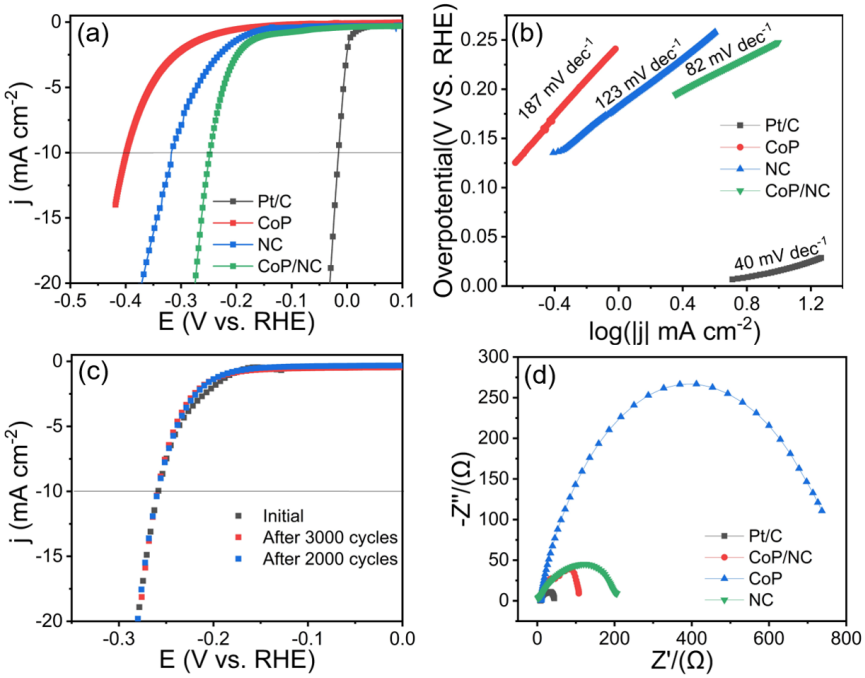

Figure S7. (a) LSV curves and (b) Tafel plots of CoP/NC, CoP, Pt/C and NC, (f) Polarization curves of CoP/NC before and after 3000 cycles; (e) Nyquist plots of CoP/NC, Pt/C, CoP and NC in 1 M KOH.

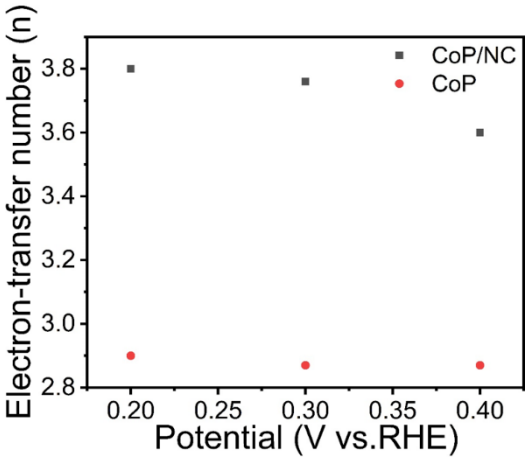

Figure S8. The electron transfer number of CoP/NC and pure CoP in 0.1 M KOH.

ACKNOWLEDGEMENTS
The authors acknowledge the financial support of Innovation and Entrepreneurship Training program for College students (2020101480009) and Scientific Research Project of the Department of Education of Liaoning Province (L2019043).

References

1. J. Song, C. Zhu, B.Z. Xu, S. Fu, M.H. Engelhard, R. Ye, D. Du, S.P. Beckman, Y. Lin, *Adv. Energy Mater.*, 7 (2017) 1601555.
2. Y. Qi, Q. Zhang, S. Meng, D. Li, W. Wei, D. Jiang, M. Chen, *Electrochim. Acta,* 334 (2020) 135633.
3. Y. Jing, H. Liu, R. Yan, J. Chen, H. Dai, C. Liu, X.D. Zhang, *ACS Appl. Nano Mater*., 2 (2019) 5922.
4. S. Zhao, Q. Wang, S. Dong, J. Chen, S. Wang, *Chem. Eng. J.*, 401 (2020) 126156.
5. J.T. Ren, L. Chen, D.D. Yang, Z.Y. Yuan, *Appl. Catal*., B, 263 (2020) 118352.
6. S. Wu, M. Chen, W. Wang, J. Zhou, X. Tang, D. Zhou, C. Liu, *Carbon*, 171 (2021) 385.
7. S. Zhao, J. Berry-Gair, W. Li, G. Guan, M. Yang, J. Li, F. Lai, F. Cora, K. Holt, D.J.L. Brett, G. He, I.P. Parkin, *Adv. Sci*., 7 (2020) 1903674.
8. Y. Zhang, H. Ren, T. Gao, J. Mou, Y. Meng, G. Tan, J. Ma, D. Xiao, *Mater. Today Energy*, 17 (2020) 100477.
9. J. W. Shi, Y. Zou, L. Cheng, D. Ma, D. Sun, S. Mao, L. Sun, C. He, Z. Wang, *Chem. Eng. J.*, 378 (2019) 122161.
10. C. Lin, P. Wang, H. Jin, J. Zhao, D. Chen, S. Liu, C. Zhang, S. Mu, *Dalton Trans*., 48 (2019) 16555.
11. K. Zhang, Z. Zhu, J. Lin, R. Zhang, C. Zhao, *Appl. Surf. Sci*., 500 (2020) 144055.
12. S. Chen, X. Yang, X. Tong, F. Zhang, H. Zou, Y. Qiao, M. Dong, J. Wang, W. Fan, *ACS Appl. Mater. Interfaces*, 12 (2020) 34971.
13. H. Tabassum, W. Guo, W. Meng, A. Mahmood, R. Zhao, Q. Wang, R. Zou, *Adv. Energy Mater*., 7 (2017) 1601671.
14. Y. Shi, B. Zhang, *Chem. Soc. Rev*., 45 (2016) 1529.
15. M. Liu, L. Yang, T. Liu, Y. Tang, S. Luo, C. Liu, Y. Zeng, *J. Mater. Chem*. A, 5 (2017) 8608.
16. M.Q. Wang, C. Ye, H. Liu, M. Xu, S.J. Bao, Angew. Chem., *Int. Ed. Engl*., 57 (2018) 1963.
17. G. L. Tian, Q. Zhang, B. Zhang, Y.G. Jin, J.Q. Huang, D.S. Su, F. Wei, *Adv. Funct. Mater*., 24

(2014) 5956.
18. A. Joshi, G. Singh, R.K. Sharma, *Chem. Eng. J*., 384 (2020) 123364.
19. Y. Zhang, Y. Wang, T. Wang, N. Wu, Y. Wang, Y. Sun, L. Fu, Y. Du, W. Zhong, *Adv. Mater. Interfaces*, 7 (2019) 1901302.
20. X. Miao, R. Yin, X. Ge, Z. Li, L. Yin, *Small*, 13 (2017) 1702138.
21. L. Yan, B. Zhang, J. Zhu, Y. Li, P. Tsiakaras, P. K. Shen, *Appl. Catal*., B, 265 (2020) 118555.
22. A.B. Jorge, R. Jervis, A.P. Periasamy, M. Qiao, J. Feng, L.N. Tran, M.M. Titirici, *Adv. Energy Mater.*, 10 (2019) 1902494.
23. X. Wang, A. Vasileff, Y. Jiao, Y. Zheng, S.Z. Qiao, *Adv. Mater*., 31 (2019) 1803625.
24. H. Jiang, J. Gu, X. Zheng, M. Liu, X. Qiu, L. Wang, W. Li, Z. Chen, X. Ji, J. Li, *Energy Environ. Sci.*, 12 (2019) 322.
25. H. Deng, Q. Li, J. Liu, F. Wang, *Carbon*, 112 (2017) 219.
26. X. Kong, Y. Huang, Q. Liu, *Carbon*, 123 (2017) 558.
27. J. Shi, F. Qiu, W. Yuan, M. Guo, Z.-H. Lu, *Chem. Eng. J*., 403 (2021)126312.
28. J. Ma, M. Wang, G. Lei, G. Zhang, F. Zhang, W. Peng, X. Fan, Y. Li, *Small*, 14 (2018) 1702859.
29. H. Huang, C. Du, S. Wu, W. Song, *J. Phys. Chem*. C, 120 (2016) 15707.
30. H. Huang, X. Feng, C. Du, S. Wu, W. Song, *J. Mater. Chem*. A, 3 (2015) 4976.
31. X.H. Li, S. Kurasch, U. Kaiser, M. Antonietti, *Angew. Chem., Int. Ed. Engl*., 51 (2012) 9689.
32. T. Meng, Y.N. Hao, L. Zheng, M. Cao, *Nanoscale*, 10 (2018) 14613.
33. R. Qin, H. Wan, X. Liu, G. Chen, N. Zhang, R. Ma, G. Qiu, *Inorg. Nano-Met. Chem*., 6 (2019) 1744.
34. Y. Men, P. Li, F. Yang, G. Cheng, S. Chen, W. Luo, *Appl. Catal*., B, 253 (2019) 21.
35. K. Chang, W. Chen, L. Ma, H. Li, H. Li, F. Huang, Z. Xu, Q. Zhang, J.Y. Lee, *J. Mater. Chem*. A, 21 (2011) 6251.
36. Z. Wang, K. Dong, D. Wang, S. Luo, X. Liu, Y. Liu, Q. Wang, Y. Zhang, A. Hao, C. He, C. Shi, N. Zhao, *Chem. Eng. J.*, 384 (2020) 123327.
37. C. Huang, D. Wu, P. Qin, K. Ding, C. Pi, Q. Ruan, H. Song, B. Gao, H. Chen, P.K. Chu, *Nano Energy*, 73 (2020) 104788.
38. H. Li, F. Ke, J. Zhu, *Nanomaterials* (Basel), 8 (2018) 89.
39. X. Guo, J. Liang, L. Wang, Z. Feng, T. Yu, Z. Zhang, Y. Shao, C. Hao, G. Li, *Int. J. Hydrogen Energy*, 43 (2018) 2034.
40. X. Huang, Q. Wang, D. Jiang, Y. Huang, *Catal. Commun*., 100 (2017) 89.
41. J.G. Li, K. Xie, H. Sun, Z. Li, X. Ao, Z. Chen, K.K. Ostrikov, C. Wang, W. Zhang, *ACS Appl. Mater. Interfaces*, 11 (2019) 36649.
42. C. Wang, J. Jiang, X. Zhou, W. Wang, J. Zuo, Q. Yang, *J. Power Sources*, 286 (2015) 464.
43. C. Wu, Y. Yang, D. Dong, Y. Zhang, J. Li, *Small*, 13 (2017) 1602873.
44. G. Yuan, J. Bai, L. Zhang, X. Wang, Y. Zhu, S. Wu, L. Ren, *ChemistrySelect*, 6 (2021) 7068.
45. J. Zhang, X. Liang, X. Wang, Z. Zhuang, *Mater. Lett*., 202 (2017) 146.
46. M. Li, X. Liu, Y. Xiong, X. Bo, Y. Zhang, C. Han, L. Guo, *J. Mater. Chem*. A, 3 (2015) 4255.
47. L. Gao, S. Chen, H. Zhang, Y. Zou, X. She, D. Yang, Q. Zhao, X. Zhao, *Int. J. Hydrogen Energy*, 43 (2018) 13904.
48. Y. Du, Z. Wang, H. Li, Y. Han, Y. Liu, Y. Yang, Y. Liu, L. Wang, *Int. J. Hydrogen Energy*, 44 (2019) 19978